ICAS 2021 SHANG HAI
International Council of the Aeronautical Sciences
32nd Congress of the International Council of the Aeronautical Sciences
September 6-10, 2021
Pudong Shangri-La, Shanghai, China

COMPUTATIONAL STUDY OF THREE-DIMENSIONAL OPEN CAVITY FLOWS

Yong Luo[1], Conghai Wu[*,1], Siqi Yuan[1], Hao Tian[1], Hu Li[1] & Shuhai Zhang[1]

[1]State Key Laboratory of Aerodynamics, China Aerodynamics Research and Development Center, Mianyang Sichuan 621000, China.
Email: wraiment@163.com

Abstract

The three-dimensional rectangular cavity with length to depth to width of 6:2:1 were simulated numerically using Spalart-Allmaras Improved Delayed Detached Eddy Simulation (SA-IDDES) method for both subsonic and supersonic flow. The self-adaptive hybrid scheme based on the Roe scheme was used for the spatial convective terms. The implicit LU-SGS was used for time advancing. The results showed the shear layer would rolls-up because of the Kelvin-Helmholtz instability of the fluids. The three-dimensional characteristic could be observed in the downstream region. The pressure signals on cavity wall were analysed by continuous wavelet transform (CWT) method. The mode-switching phenomenon was identified for both subsonic and supersonic case for the present cavity configuration.

Keywords: cavity, acoustic, mode-switching

1. Introduction

Cavity is a typical configuration which is widely used in aeronautic aircrafts. The flow past an open cavity involves many complex phenomena such as resonant tones, shear layer instabilities, complex wave interactions, even including shock wave in supersonic flow. The noise radiated by the cavity has been widely studied for decades due to its important values both on theory and applications. These intense resonant tones could fatigue nearby components and cause security problems[1]. A clear understanding of the fundamental mechanisms underlying cavity flow oscillations will help us to find effective strategies to suppress these resonant tones, which is still a challenge today. Thus, numerous researchers have made effort to identify the mechanism and develop various theoretical models on the issue[2–4]. The most important physical mechanism of the cavity oscillations proposed by Rossiter[5] is the flow/acoustic resonance, described as follows: (i) Kelvin-Helmholtz instability excites an unstable shear layer and generates vortex, (ii) the shear layer moves downstream and impinge on the back wall, which generates acoustic waves that propagate upwards, (iii) the acoustic waves interacts with the leading edge fluids and further excites the shear layer instabilities. The idea of such a feedback loop was known earlier for edge-tones in Powell's work[6, 7]. Through a series of experimental tests, Krishnamurty[8] discovered that the subsonic and supersonic flows past rectangular cavities would emit a strong acoustic radiation. Rossiter[5] identified a series oscillating modes with different discrete frequencies and gave a semi-empirical formula to predict the resonant frequencies.

In three-dimensional cavities, the flow and acoustic resonance may generates a series Rossiter modes, which could be identified as the peaks from the time-averaged power spectra. To suppress these modes using control theory, it must be ascertained whether these modes coexist independent or not. Kegerise *et al.*[9–12] conducted experiments for Mach numbers ranging from 0.2 to 0.6 with $L/D = 2$ and $L/D = 4$. They found the dominant mode of the cavity oscillations switches between the primary Rossiter modes. Xavier[13] performed a numerical simulation for Mach number 0.8 with

$L/D = 3$ and found the switching between Rossiter mode I and Rossiter mode II of cavity oscillations. However, they simulation used periodic boundary conditions in the spanwise direction which is different from the real configurations. Recently, Thangamani[14] studied the behavior of the oscillation modes in supersonic flow for Mach number 1.58 with $L/D = 2$ from experiments, and also observed the mode switching between the first and second modes of oscillation. However, the size of the cavities are different from the above studies in some engineering applications. The length to depth of these cavities is always between 4 to 10[15] and the shear layer above the cavity would develop more sufficiently than the short cavities. Especially, the three-dimensional effect is intense at the downstream with the turbulent incoming flow. Thus, the cavities with this condition requires more studies since the behavior of the cavity oscillating modes may be affected by the strong three-dimensional characteristic.

In this paper, we try to identify the behavior of the cavity oscillating modes numerically for the three-dimensional rectangular cavities with length to depth to width of 6:2:1. In section 2, we present the numerical method for solving the URANS equations in three-dimensional cavity and the validation of computational results. In section 3, the fluid structures are analyzed to show the three-dimensional characteristic, and the pressure perturbation signals in cavity are analyzed by the fast fourier transform (FFT) and CWT methods. We give the conclusion in section 4.

2. Numerical Simulations

2.1 Numerical Method and Flow Configuration

The three-dimensional rectangular cavity are solved numerically with the SA-IDDES[16] method using a finite volume solver. The spatial convective terms is calculted by the self-adaptive hybrid scheme based on the Roe scheme[17],

$$\boldsymbol{F} = \frac{1}{2}\left(\boldsymbol{F}_L + \boldsymbol{F}_R\right) + \sigma\left(\frac{1}{2}|\tilde{\boldsymbol{A}}|(\boldsymbol{U}_R - \boldsymbol{U}_L)\right) \tag{1}$$

where, $\boldsymbol{F}_L$, $\boldsymbol{F}_R$, $\boldsymbol{U}_L$, $\boldsymbol{U}_R$, $\tilde{\boldsymbol{A}}$ and σ are the left flux, right flux, left primitive variables, right primitive variables, Roe averaged matrix and the hybrid weight function. The primitive variables on the interface of each cell is reconstructed by a third order method. The σ is the hybrid weighted function to adjust the dissipation[18, 19],

$$\sigma = \min(1, \max(\sigma_1, \sigma_{\min})), \quad \sigma_{\min} = 0.03 \tag{2}$$

The details of the formula σ_1 could be found in Travin *et al.*'s work[19]. We use the implicit LU-SGS[20] method for time discretion.

In this paper, the cavity size is chose according to the experimental model designed by High Speed Aerodynamics Research Institute of China Aerodynamics Research and Development Center (CARDC)[21]. The length, width and depth of the cavity are $L = 200mm$, $W = 66.67mm$ and $D = 33.33mm$, respectively ($L : W : D = 6 : 2 : 1$). A schematic diagram of the cavity configuration is shown in figure 1. The origin of coordinate system is at the leading edge of the central plane of the cavity, the X-axis, Y-axis and Z-axis are the transverse, longitudinal and spanwise direction, respectively. A cartesian stretched grid which is dense near the wall and sparse in the far field region is used. The total number of grids is about 16 million, and the minimum grid spacing is $1.0 \times 10^{-4}D$. Figure 2 shows a part of grids on the spanwise central plane. The wall is assumed to be adiabatic. All variables are non-dimensionalized by the reference density ρ_∞, the reference temperature $T_\infty = 288.15K$, the cavity depth D and the flow velocity U_∞ respectively. Here, the subscript ∞ represents the flow parameters at infinity. The Mach number Ma and the Reynolds number Re are constants related to specific computational cases. Table 1 shows the computational parameters for different Mach numbers. All simulations are performed by the NNW-PHengLei software[22] developed by Computational Aerodynamics Institute of CARDC.

2.2 Validation

The overall sound pressure level (OASPL) represents the intense of oscillation in cavity, which defined as,

$$\mathrm{OASPL} = 20\log_{10}\left(\frac{p_{\mathrm{e}}}{P_{\mathrm{ref}}}\right) \tag{3}$$

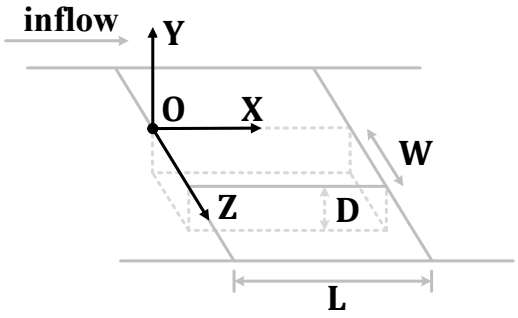

Figure 1 – Schematic diagram of the cavity configuration.

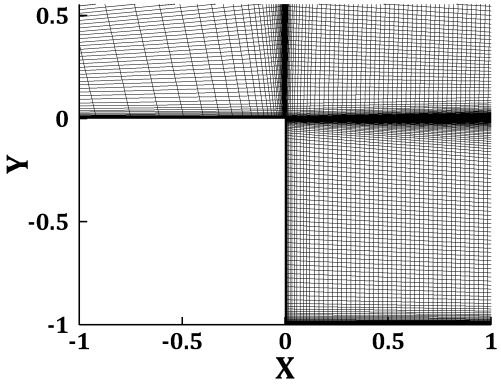

Figure 2 – A part of grids on the spanwise central plane.

Case	Ma	Pressure (Pa)	Temperature (K)	Re
B6	0.6	102613	268.66	4.04×10^5
B9	0.9	67938.3	247.85	5.68×10^5
SO5	1.5	38080.2	198.62	7.13×10^5
ST2	2.0	23862.0	160.00	8.04×10^5

Table 1 – The computational parameters for different cases (The Re is based on the depth of the cavity).

here, p_e can be calculated by,

$$p_e = \sqrt{\sum_{i=1}^{N} \left(p - \bar{P}\right)^2 \Big/ N} \tag{4}$$

where $\bar{P}$ is the averaged pressure, and $P_{ref} = 2 \times 10^{-5}$Pa is the reference pressure that represents the hearing threshold value of sound of 1kHz.

Figure 3 shows the OASPL of the present numerical result and their comparison with the experimental result of Yang *et al.*[21] for Mach number 0.9. The maximum difference of the OASPL between the computation and experiment is less than 2dB, and the averaged error of the OASPL for different locations in cavity is 1.5dB.

The power spectral density (PSD) of the pressure perturbation signal represents the intense of different frequencies of the oscillations in cavity. The PSD converts to the SPL as follows,

$$\mathrm{SPL} = 10 \log_{10} \left(\frac{\mathrm{PSD}}{P_{ref}^2} \right) \tag{5}$$

where P_{ref} is the reference pressure as mentioned above. Figure 4 contains the spectra of the pressure perturbation signals on the leading wall and their comparisons with the experiment[21]. The PSD was computed using Burg Autoregressive method. It can be noted that the frequency of the most energetic peaks in spectra are agree well with the experimental results. Thus, the present numerical methods can be used to predict the characteristics of the cavity flow.

3. Results and Discussion

3.1 Fluid Structures

Figure 5 shows the vorticity contours and the time-averaged streamlines on the central plane for four Mach numbers. The recirculation zone is shown clearly in both the subsonic and supersonic case. The core of the recirculation zone is located near the center of the cavity. It is not strange that the core for the supersonic case is closer to the back wall than the subsonic case, since the impingement between the shear layer and the back wall is more powerfully as the Mach number increases and the vortex would rolls-up more easily. Figure 6 is the mean C_p along the cavity floor central line of

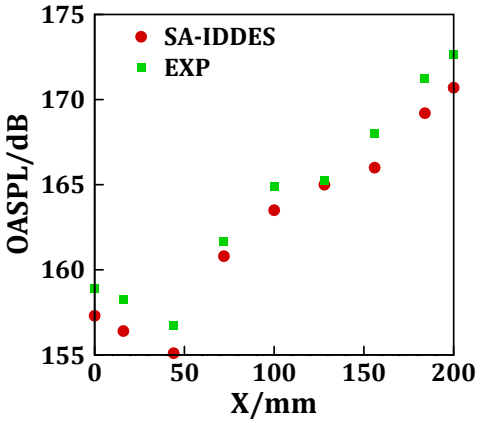

Figure 3 – $\mathrm{Ma} = 0.9$, comparison between the experiment[21] and the present numerical results of OASPL at different locations in cavity

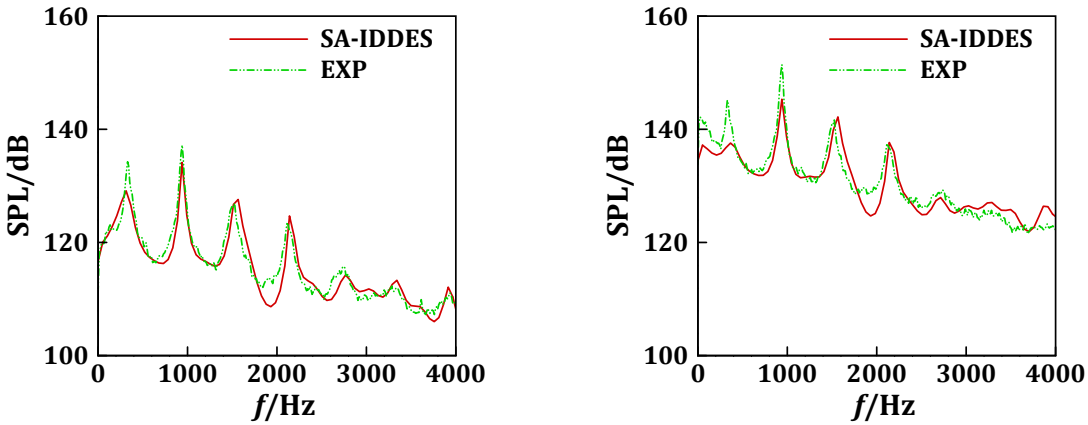

(a) $(x, y, z) = (0, -0.88, 1)D$ (b) $(x, y, z) = (6, -0.88, 1)D$

Figure 4 – $\mathrm{Ma} = 0.9$, comparisons between the experiment[21] and the present numerical results of the spectra of the pressure perturbation signals at the front and back wall of the cavity.

four cases. For the subsonic cases, the mean C_p profile has a lower value region at the center of the cavity due to the movement of the core vortex. This low pressure region is similar to the experimental result of the incompressible flow[23]. For the supersonic cases, the lower value region of the mean C_p are unconspicuous. In Rowley's study[24] of two-dimensional cavities, a new regime called wake mode may present as the length or depth of the cavity or Mach and Reynolds numbers increases. Its time-averaged streamlines are significantly deflected above the cavity as shown in figure 18(b) of Rowley's paper[24]. Gharib and Roshko[25] first observed wake mode in an axisymmetric water cavity experiment. The flow contains a phenomenon that the vortex shedding behind bluff bodies resembles the wake. However, wake mode can not be observed in experiments of compressible cavity flows. The numerical studies performed by Shieh and Morris[26, 27] indicate that it is related to the two-dimensional nature of the bifurcation. The present numerical results for subsonic and supersonic cases also support this conclusion. The development of the shear layer also can be noted in figure 5. The flow separates at the front wall and forms the shear layer. The shear layer lose its stability due to the Kelvin-Helmholtz instability of the fluids. The vortex rolls-up in the shear layer and impinges on the back wall. The vorticity contours clearly show that the shear layer develop sufficiently especially in the downstream region. In this process, the fluids would be injected into the cavity periodically and form the recirculation zone. The oscillations in cavity are directly related to this periodic fluids injection.

Figure 7 is the iso-surface of Q-value contours represents the vortical structures[28]. For both the subsonic and supersonic cases, the transition of the shear layer from two-dimensional to three-

dimensional are shown clearly. Once this transition is complete, the hairpin vortices are generated in the shear layer. These hairpin vortices are highly asymmetric, especially in the downstream region. These asymmetry is identified by the slices of Q-value of fluid field for both the subsonic and supersonic cases in figure 8. According to the Crook *et al.*[29]'s research, there is a single tornado vortex that located near the cavity centreline at the front of the cavity. This tornado vortex may cause the asymmetry in the instantaneous flow field. It can be seen from figure 7a and 7b that the vertical fluctuation is stronger for the Mach number 0.9 case than the Mach number 1.5 case. This phenomenon also shown in figure 5, and there are more small vortices for the Mach number 1.5 case. These suggest that the shear layer presents stronger two-dimensional characteristic for the Mach number 0.9 case.

3.2 Frequencies Features

With the turbulent incoming flow and the three-dimensional configuration, the spectra of the pressure perturbation signals contain several peaks that represent different oscillation modes. These peaks would be modulated by the Rossiter modes and the low frequency component caused by the three-dimensional effect. Figure 9 are the CWT results of the pressure perturbation signal at the front wall in cavity for different Mach numbers. Its vertical axis is the non-dimensional frequency (Strouhal numbers). Although the Rossiter modes are different for different Mach numbers, the mode-switching phenomenon is shown clearly in all cases. For Mach number 0.6, the main components are Rossiter mode 1, 3 and 5. For Mach number 0.9 and 1.5, the main components are Rossiter mode 1, 2 and 3. For Mach number 2.0, the main components are Rossiter mode 1, 2 and 6. We extract these components from the CWT results to identify the time-developing details of the main Rossiter modes. The results are shown in figure 10. The switching phenomenon between the dominant mode and the subdominant mode is further identified. However, the higher Rossiter mode presents more sophisticated characteristic. Take the Mach number 0.9 for example, the Rossiter mode 3 presents competitive in energy with the dominant Rossiter mode 2. But its tendency presents similarity with the subdominant Rossiter mode 1. Besides, this higher Rossiter mode fluctuates more strongly.
According to the theory of shear layer stability, the thickness of the incoming boundary layer was recognized as a determinant factor for the mode selection[30]. This is also shown by Gharib *et al.*[31] and Rowley *et al.*[24], they found that the cavity length over the boundary-layer thickness is an important factor to the mode selection. Figure 11 shows the time trace of the boundary-layer momentum thickness at the leading edge of the central plane ($(x, y, z) = (0, 0, 1)D$) and its CWT analysis result for Mach number 0.9. It can be noted from figure 11b that the result is similar to the CWT result of the pressure signals in the wall (figure 9b). The main frequencies components are also Rossiter mode 1, 2 and 3. In our study of the two-dimensional cavity flow for subsonic and supersonic cases[32], the boundary-layer momentum thickness fluctuations are similar to the pressure signals at the solid wall in cavity. The present three-dimensional results further identify the flow/acoustic resonance mechanism of the cavity oscillations[5].

4. Conclusion

We have used the SA-IDDES method to investigate the flow past a three-dimensional rectangular cavity of $L : W : D = 6 : 2 : 1$ for both the subsonic and supersonic cases. The results of the fluids structure shows, the development of the shear layer is sufficient with the present configuration, and the flow contains the obvious three-dimensional effect. The three-dimensional asymmetry has also be observed. In addition, we found that the shear layer presents stronger two-dimensional characteristic for the Mach number 0.9 than Mach number 1.5. The pressure perturbation signals at the front wall of the cavity have been analyzed by the CWT method. The results shows, there is a mode-switching phenomenon between the dominant mode and the subdominant mode. However, the evolution details of each mode are complicated, the higher Rossiter modes fluctuate more strongly. Especially, the amplitudes of these high order modes are very high at certain periods. This sophisticated feature may bring additional challenges to the research of the noise reduction methods for the cavity flow.

Acknowledgement

This research was partially supported by the National Numerical Windtunnel project. Research of the final author is supported by the National Natural Science Foundation of China with the grant No. 11732016 and Sichuan Science and Technology Program with the grant No. 2018JZ0076.

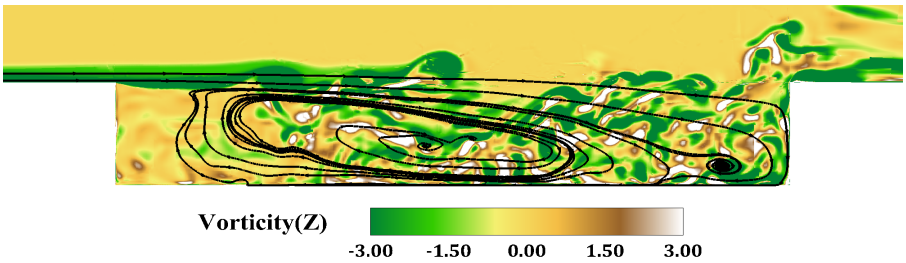

(a) Ma = 0.6

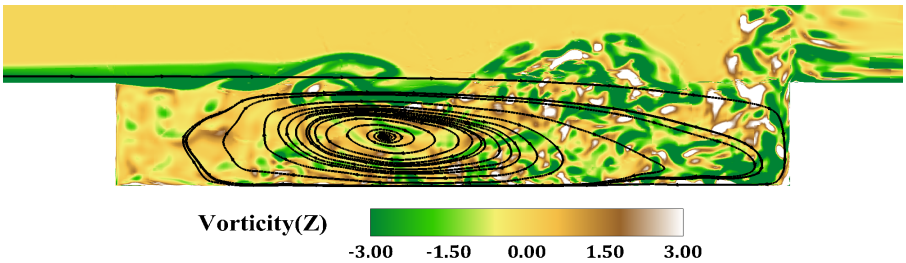

(b) Ma = 0.9

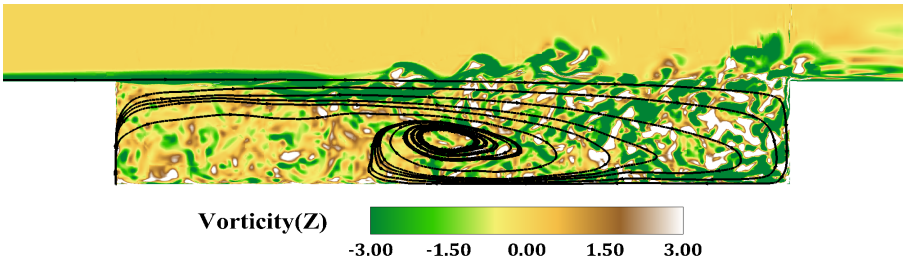

(c) Ma = 1.5

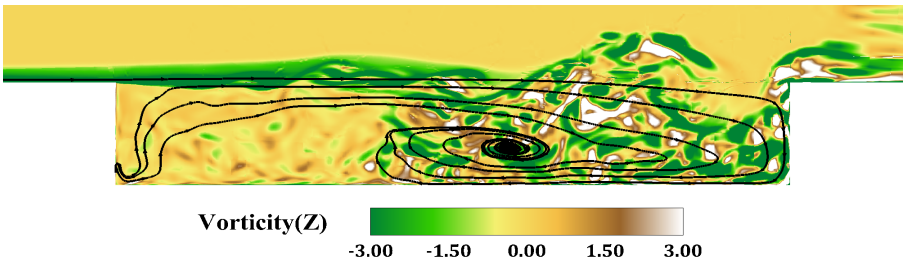

(d) Ma = 2.0

Figure 5 – The vorticity contours and the time-averaged streamlines on the central plane for the subsonic and supersonic case.

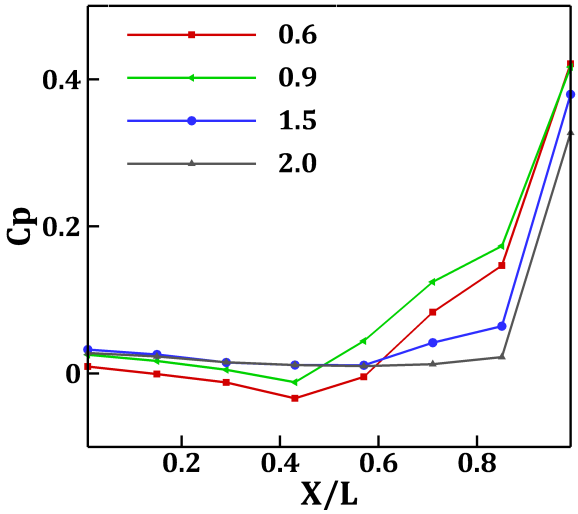

Figure 6 – The mean C_p along the cavity floor central line of different Mach numbers

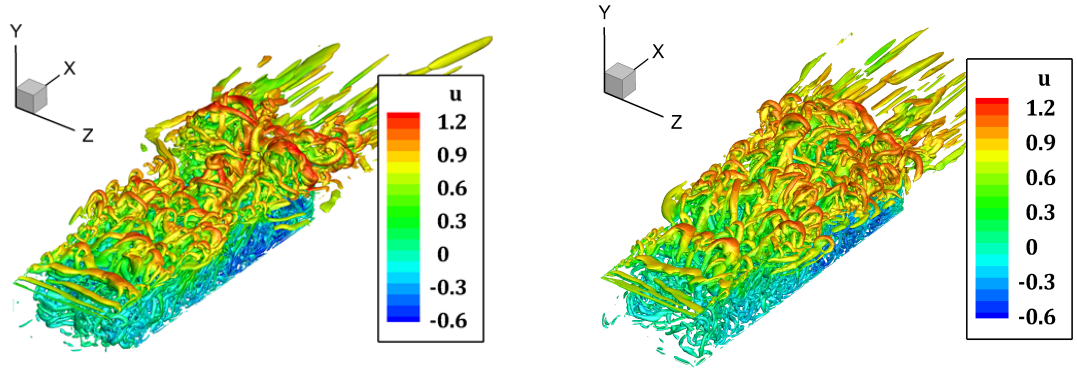

(a) Ma = 0.9 (b) Ma = 1.5

Figure 7 – The iso-surface ($Q = 1$) of Q-value of fluid field for the subsonic and supersonic case.

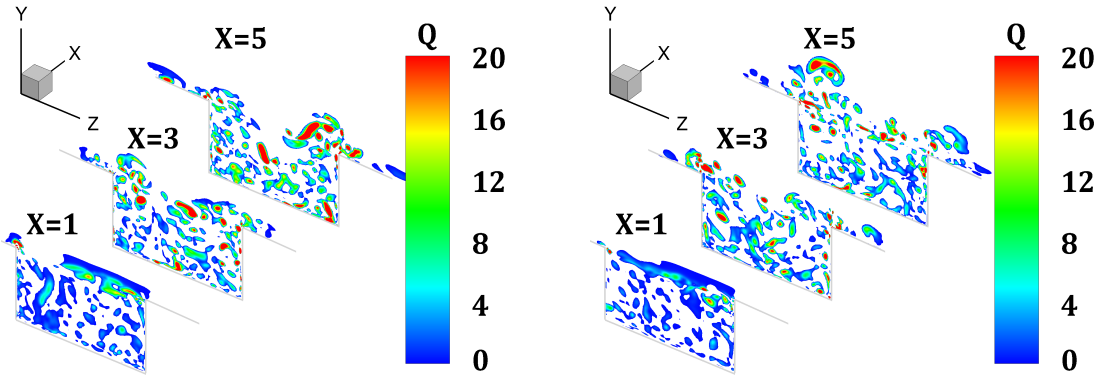

(a) Ma = 0.9 (b) Ma = 1.5

Figure 8 – The slices of Q-value of fluid field for the subsonic and supersonic case.

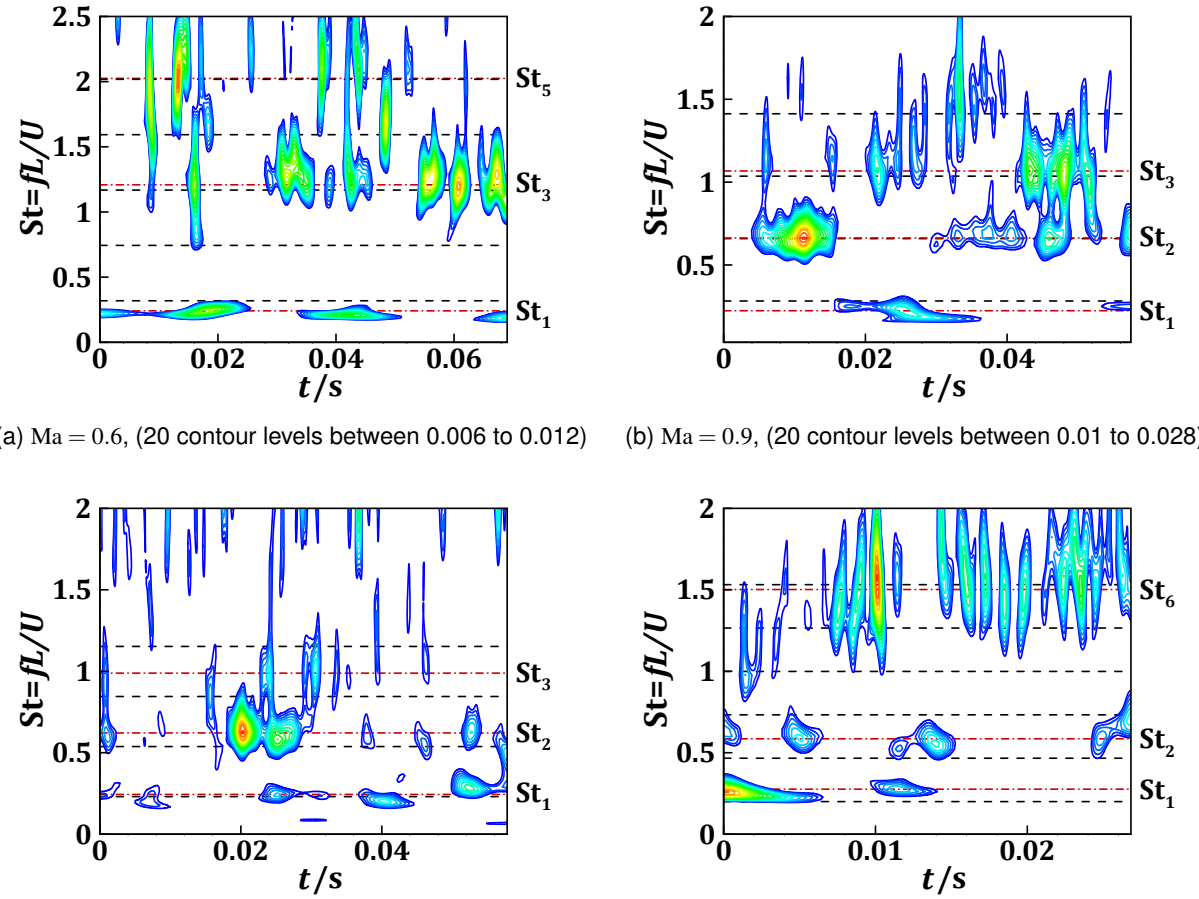

(a) $\mathrm{Ma} = 0.6$, (20 contour levels between 0.006 to 0.012)

(b) $\mathrm{Ma} = 0.9$, (20 contour levels between 0.01 to 0.028)

(c) $\mathrm{Ma} = 1.5$, (20 contour levels between 0.006 to 0.02)

(d) $\mathrm{Ma} = 2.0$, (20 contour levels between 0.007 to 0.018)

Figure 9 – The CWT results of the pressure perturbation signal on cavity wall $((x,y,z) = (0,-0.88,1)D)$ for different Mach numbers. Rossiter's semi-empirical formula: horizontal dashed line (– – – –); the dominant frequencies: dashdot line (– · – ·).

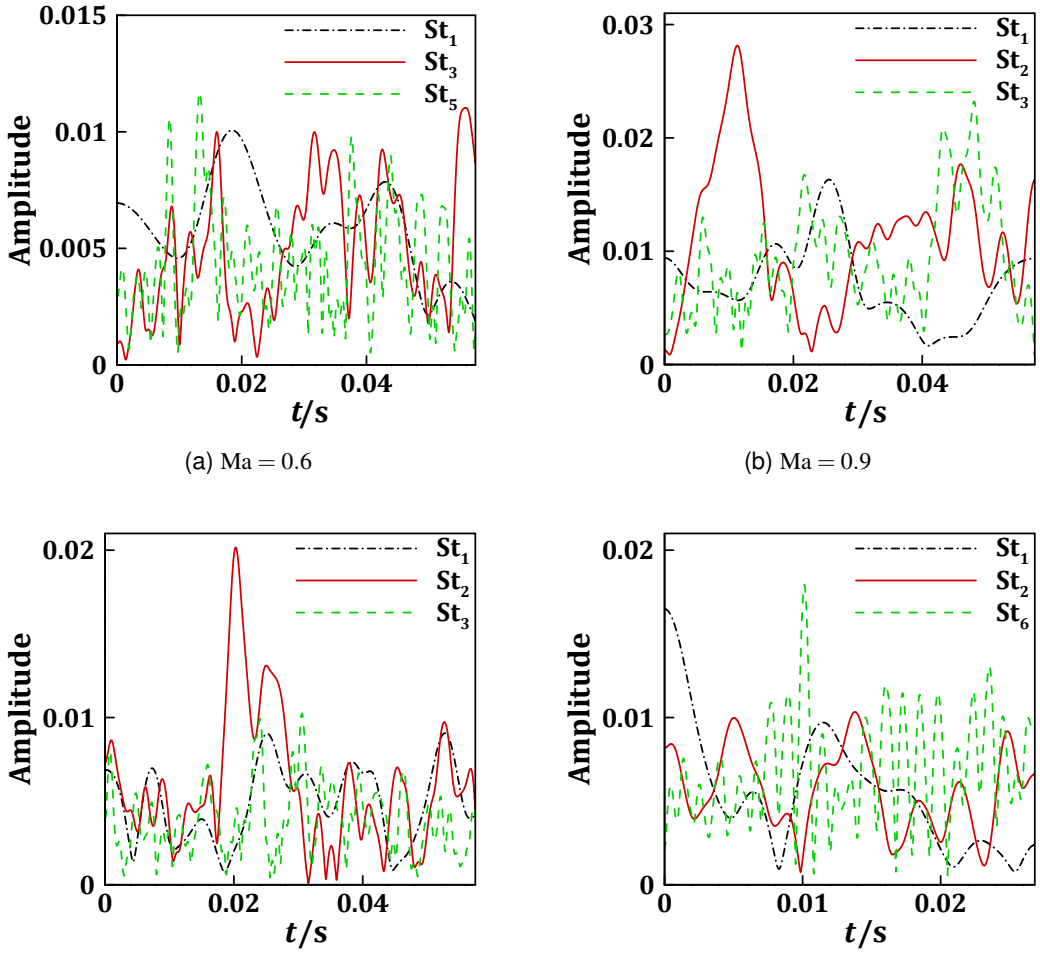

Figure 10 – The dominant modes extracted from the CWT result for different Mach numbers.

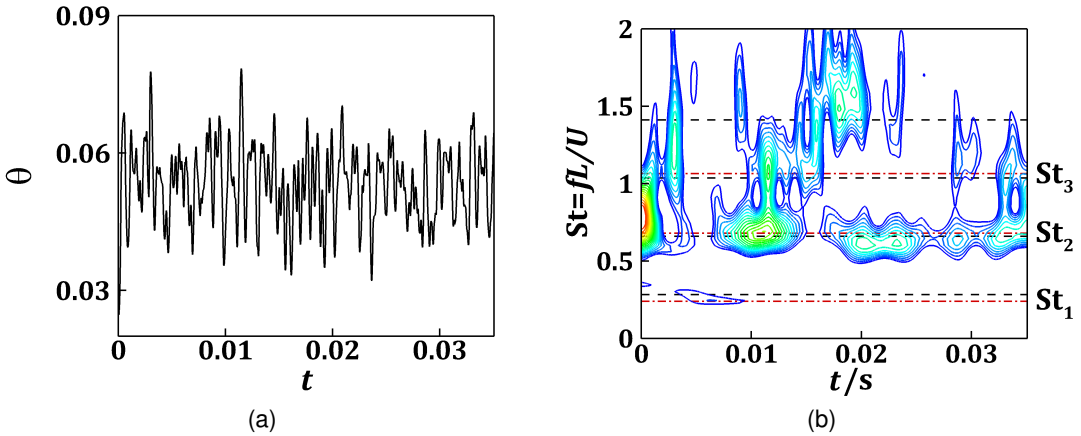

Figure 11 – Ma = 0.9, (a) time trace of the boundary-layer momentum thickness at the leading edge, (b) the CWT result of (a).

References

[1] Morton, M. H., Certification of the F-22 Advanced Tactical Fighter for High Cycle and Sonic Fatigue, *AIAA Paper*, , No. 2007-1766, 2000.

[2] Colonius, T., An overview of simulation, modeling, and active control of flow/acoustic resonance in open cavities, *AIAA Paper*, , No. 2001-0076, 2001.

[3] Gloerfelt, X., Bogey, C., and Bailly, C., Cavity noise, Arts et Métiers ParisTech, France, 2007. https://doi.org/10.1017/CBO9780511546143.014.

[4] Sinha, J., and Arora, K., Review of the flow-field analysis over cavities, 2017, pp. 870–876.

[5] Rossiter, J. E., Wind-Tunnel Experiments on the Flow over Rectangular Cavities at Subsonic and Transonic Speeds, *Aeronautical Research Council Reports and Memoranda*, Vol. No. 3438(1964), 1964.

[6] Powell, A., On edge tones and associated phenomena, *Acta Acustica United with Acustica*, Vol. 3, 1953, pp. 233–243.

[7] Powell, A., On the Edgetone, *The Journal of the Acoustical Society of America*, Vol. 33, No. 4, 1961, pp. 395–409.

[8] Krishnamurty, K., Sound radiation from surface cutouts in high speed flow, Ph.D. thesis, California Institute of Technology, Pasadena, California, 1956.

[9] Cattafesta, L., Garg, S., Kegerise, M., and Jones, G., Experiments on compressible flow-induced cavity oscillations, *AIAA Paper*, , No. 1998-2912, 1998.

[10] Garg, S., and Cattafesta, L., Quantitative schlieren measurements of coherent structures in a cavity shear layer, *Experiments in Fluids*, Vol. 30, No. 2, 2001, pp. 123–134.

[11] Kegerise, M. A., Cabell, R. H., and Cattafesta, L. N., Real-Time Adaptive Control of Flow-Induced Cavity Tones (Invited), *AIAA Paper*, , No. 2004-0572, 2004.

[12] Kegerise, M. A., Spina, E. F., Garg, S., and Cattafesta, L. N., Mode-switching and nonlinear effects in compressible flow over a cavity, *Physics of Fluids*, Vol. 16, No. 3, 2004, pp. 678–687.

[13] Gloerfelt, X., Bogey, C., and Bailly, C., Numerical evidence of mode switching in the flow-induced oscillations by a cavity, *International Journal of Aeroacoustics*, Vol. 2, No. 2, 2003, pp. 193–217.

[14] Thangamani, V., Mode Behavior in Supersonic Cavity Flows, *AIAA Journal*, Vol. 57, No. 8, 2019, pp. 3410–3421.

[15] Guo, Q., Numerical Simulations and Physical Analyses of the Complex Turbulent Flow and Aerodynamic Noise in Cavities, Ph.D. thesis, China Aerodynamics Research and Development Center Graduate School, Mianyang, China, 2017.

[16] Shur, M. L., Spalart, P. R., Strelets, M. K., and Travin, A. K., A Hybrid RANS-LES Approach with Delayed-DES and Wall-Modelled LES Capabilities, *International Journal of Heat and Fluid Flow*, Vol. 29, No. 6, 2008, pp. 1638–1649.

[17] Roe, P., Approximate Riemann Solvers, Parameter Vectors, and Difference Schemes, *Journal of Computational Physics*, Vol. 135, No. 2, 1997, pp. 250–258.

[18] Yang, Z., Laiping, Z., Xin, H., and Xiaogang, D., An improved second-order finite-volume algorithm for detached-eddy simulation based on hybrid grids, *Communications in computational physics*, Vol. 20, No. 2, 2016, pp. 459–485.

[19] Travin, A., Shur, M., Strelets, M., and Spalart, P. R., Physical and numerical upgrades in the detached-eddy simulation of complex turbulent flows, Berlin: Springer, 2004, pp. 239–254.

[20] Jameson, A., and Yoon, S., Lower-upper implicit schemes with multiple grids for the Euler equations, *AIAA Journal*, Vol. 25, No. 7, 1987, pp. 929–935.

[21] Yang, D.-G., Lu, B., Cai, J.-S., Wu, J.-Q., Qu, K., and Liu, J., Investigation on flow oscillation modes and aero-acoustics generation mechanism in cavity, *Modern Physics Letters B*, Vol. 32, 2018.

[22] Chen, J. Q., Advances in the key technologies of Chinese national numerical windtunnel project (in Chinese), *Sci Sin Tech*, Vol. 51, 2021.

[23] Crook, S. D., Lau, T. C. W., and Kelso, R. M., Three-dimensional flow within shallow, narrow cavities, *Journal of Fluid Mechanics*, Vol. 735, 2013, pp. 587–612.

[24] Rowley, C. W., Colonius, T., and Basu, A. J., On self-sustained oscillations in two-dimensional compressible flow over rectangular cavities, *Journal of Fluid Mechanics*, Vol. 455, No. 455, 2002, pp. 315–346.

[25] Gharib, M., and Roshko, A., The effect of flow oscillations on cavity drag, *Journal of Fluid Mechanics*, Vol. 177, 1987, pp. 501–530.

[26] Shieh, C. M., and Morris, P. J., Parallel Computational Aeroacoustic Simulation of Turbulent Subsonic Cavity Flow, *AIAA Paper*, , No. 2000-1914, 2000.

[27] Shieh, C. M., and Morris, P. J., Comparison of Two- and Three-Dimensional Turbulent Cavity Flows, *AIAA Paper*, , No. 2001-0511, 2001.

[28] Hunt, J. C. R., Wray, A. A., and Moin, P., Stream and convergence zones in turbulent flows, *Center for Turbulence Research Report CTR-S88*, 1988, pp. 193–208.

[29] Crook, S. D., Lau, T. C. W., and Kelso, R. M., Three-dimensional flow within shallow, narrow cavities, *Journal of Fluid Mechanics*, Vol. 735, 2013, pp. 587–612.

[30] Tam, C. K. W., and Block, P. W., On the tones and pressure oscillations induced by flow over rectangular cavities, *Journal of Fluid Mechanics*, Vol. 89, 1978, pp. 373–399.

[31] Gharib, M., and Roshko, A., The effect of flow oscillations on cavity drag, *Journal of Fluid Mechanics*, Vol. 177, 1987, p. 501–530.

[32] Luo, Y., Li, H., Han, S., and Zhang, S., Direct Numerical Simulations of Self-Sustained Oscillations in Two-Dimensional Open Cavity for Subsonic and Supersonic Flow, *Advances in Applied Mathematics and Mechanics*, Vol. 13, No. 4, 2021, pp. 942–965.

Copyright Statement